Environmental Pollution 259 (2020) 113858

Contents lists available at ScienceDirect

Environmental Pollution

journal homepage: www.elsevier.com/locate/envpol

Use of chemical concentration changes in coastal sediments to compute oil exposure dates☆

Junfei Xia [a], Wei Zhang [b], Alesia C. Ferguson [c], Kristina D. Mena [d], Tamay M. Özgökmen [b], Helena M. Solo-Gabriele [a, *]

[a] Department of Civil, Architectural and Environmental Engineering, University of Miami, P.O. Box 248294, Coral Gables, FL, 33124-0630, USA
[b] Rosenstiel School of Marine and Atmospheric Science, University of Miami, 4600 Rickenbacker Causeway, Miami, FL 33149-1031, USA
[c] Department of Built Environment, College of Science and Technology, North Carolina Agricultural and Technical State University, 110 Price Hall, 1601 E. Market Street, Greensboro, NC, 27411, USA
[d] Department of Epidemiology, Human Genetics, & Environmental Sciences, University of Texas – Houston School of Public Health, 1200 Pressler Street, Houston, TX 77030, USA

ARTICLE INFO

Article history:
Received 13 August 2019
Received in revised form
19 December 2019
Accepted 19 December 2019
Available online 24 December 2019

Keywords:
Oil spill
Gulf of Mexico
Exposure date
Oil transportation
Chemical concentrations

ABSTRACT

Oil spills can result in changes in chemical contaminant concentrations along coastlines. When concentrations are measured along the Gulf of Mexico over time, this information can be used to evaluate oil spill shoreline exposure dates. The objective of this research was to identify more accurate oil exposure dates based on oil spill chemical concentrations changes (CCC) within sediments in coastal zones after oil spills. The results could be used to help improve oil transport models and to improve estimates of oil landings within the nearshore. The CCC method was based on separating the target coastal zone into segments and then documenting the timing of large increases in concentration for specific oil spill chemicals (OSCs) within each segment. The dataset from the Deepwater Horizon (DWH) oil spill was used to illustrate the application of the method. Some differences in exposure dates were observed between the CCC method and between oil spill trajectories. Differences may have been caused by mixing at the freshwater and sea water interface, nearshore circulation features, and the possible influence of submerged oil that is unaccounted for by oil spill trajectories. Overall, this research highlights the benefit of using an integrated approach to confirm the timing of shoreline exposure.

1. Introduction

On April 20, 2010, an explosion on the Deepwater Horizon (DWH) drilling platform (28.74°N, 88.37°W) led to an 87-day continuous and uncontrolled leak of the Macondo oil well, located approximately 65 km southeast from the nearest point on the Mississippi River Delta (Kujawinski et al., 2011, Freudenburg and Gramling, 2011; Black et al., 2016). The closest inhabited coastlines were along the Mississippi-Alabama-Florida and Louisiana-Texas shelf areas (Michel et al., 2013). The oil was visible on the sea surface on April 22, 2010 and the leak stopped after a capping stack was installed on the well July 15, 2010. The total oil released from the DWH leak was $4.4*10^6 \pm 20\%$ barrels (about 700,000 m^3) (McNutt et al., 2012). The majority of the transport was towards the coastlines in the general northern direction coupled with longshore currents (Liu et al., 2013; Özgökmen et al., 2016). The strongest tendency for southward oil transport was observed during the third week of May 2010, when oil was rapidly entrained in a loop current frontal eddy, forming a 325 km "tiger tail" pattern, shown in Fig. 2b (Smith et al., 2014; Walker et al., 2011). This southward advection was interrupted by northward winds (Le Hénaff et al., 2012), further obstructed by loop current transformations following the formation of an eddy named Franklin in late May (Hamilton et al., 2011).

Understanding oil exposure dates is important for cleanup efforts (Al-Majed et al., 2012), for mitigating damage to ecologically sensitive areas (Bae et al., 2018) and for issuing public health advisories (McCready and Williams, 2011). During cleanup efforts to facilitate rapid response, equipment and personnel are deployed to

☆ This paper has been recommended for acceptance by Bernd Nowack.

* Corresponding author.
E-mail addresses: jxx191@miami.edu (J. Xia), wei.zhang@rsmas.miami.edu (W. Zhang), acferguson@ncat.edu (A.C. Ferguson), kristina.d.mena@uth.tmc.edu (K.D. Mena), tozgokmen@rsmas.miami.edu (T.M. Özgökmen), hmsolo@miami.edu (H.M. Solo-Gabriele).

https://doi.org/10.1016/j.envpol.2019.113858
0269-7491/

areas where impacts are forecasted. Accurate exposure dates are needed to deploy measures aimed at protecting sensitive habitats and minimizing ecosystem losses. Beach areas impacted by oil spill chemicals are usually closed shortly before oil exposure dates due to potential concerns of health impacts from contact with oil. This work is motivated by the need for accurate nearshore forecasts which play an important role in oil spill response efforts and for reducing impacts to sensitive habitats and human health.

The current study was facilitated by the extensive data collected during the DWH oil spill. Oil spill forecast and exposure data included oil spill trajectories based upon an oil transport model as run by the National Oceanographic and Atmospheric Administration (NOAA) Office of Response and Restoration (OR&R) and remote sensing imagery archived by the Environmental Response Management Application-Gulf of Mexico (ERMA). Four days after the DWH explosion NOAA OR&R initiated an oil spill transport model to guide response operations. The oil spill transport model underlying these predictions was the General NOAA Oil Modeling Environment (GNOME) model (Beegle-Krause, 1999, 2001). GNOME is an interactive environmental simulation system based on following oil particles called Lagrangian elements. It was designed for the rapid modeling of pollutant trajectories in the marine environment.

In addition to trajectories from the GNOME model, satellite remote sensing, which is another key technology used for detecting and quantifying oil spills (Ganta et al., 2012; Garcia-Pineda et al., 2009, 2013; Leifer et al., 2012), was used during the DWH oil spill to track the location of the oil. As part of this effort, three days after the DWH explosion CSTARS at University of Miami started to acquire Synthetic Aperture Radar (SAR) passes for the GoM. During the active oil spill (from April to August), an extensive array of space-borne and aerial sensors was utilized in assessing the daily evolution of the spill.

In earlier studies, oil spill models and remote sensing images were the most common method used to study oil spill impact areas (Price et al., 2006; Özgökmen et al., 2014; Berta et al., 2015; Xu et al., 2016). However, this current study provides an additional method based on the chemical concentration change in sediment samples. The objective of the current research was to use changes in oil spill chemical concentrations in coastal zones to estimate the timing of oil exposure, including the earliest exposure date along the coastline. Results were compared with the output from the NOAA OR&R GNOME oil spill model and with remote sensing imagery available through ERMA. Other readily available oceanographic information including drifter data and ocean color maps were used to explain differences between the different methods.

2. Methods

This research focused on evaluating a new method based on the timing of OSC concentration changes in sediment samples collected along the coast during an active oil spill. We refer to this method as the computation of changes in concentration (CCC) method. The focus was on evaluating nearshore sediment data because chemical concentrations are not as transient as in water and concentrations tend to remain at detectable levels once impacted for longer periods after landfall. The CCC method requires comparison of

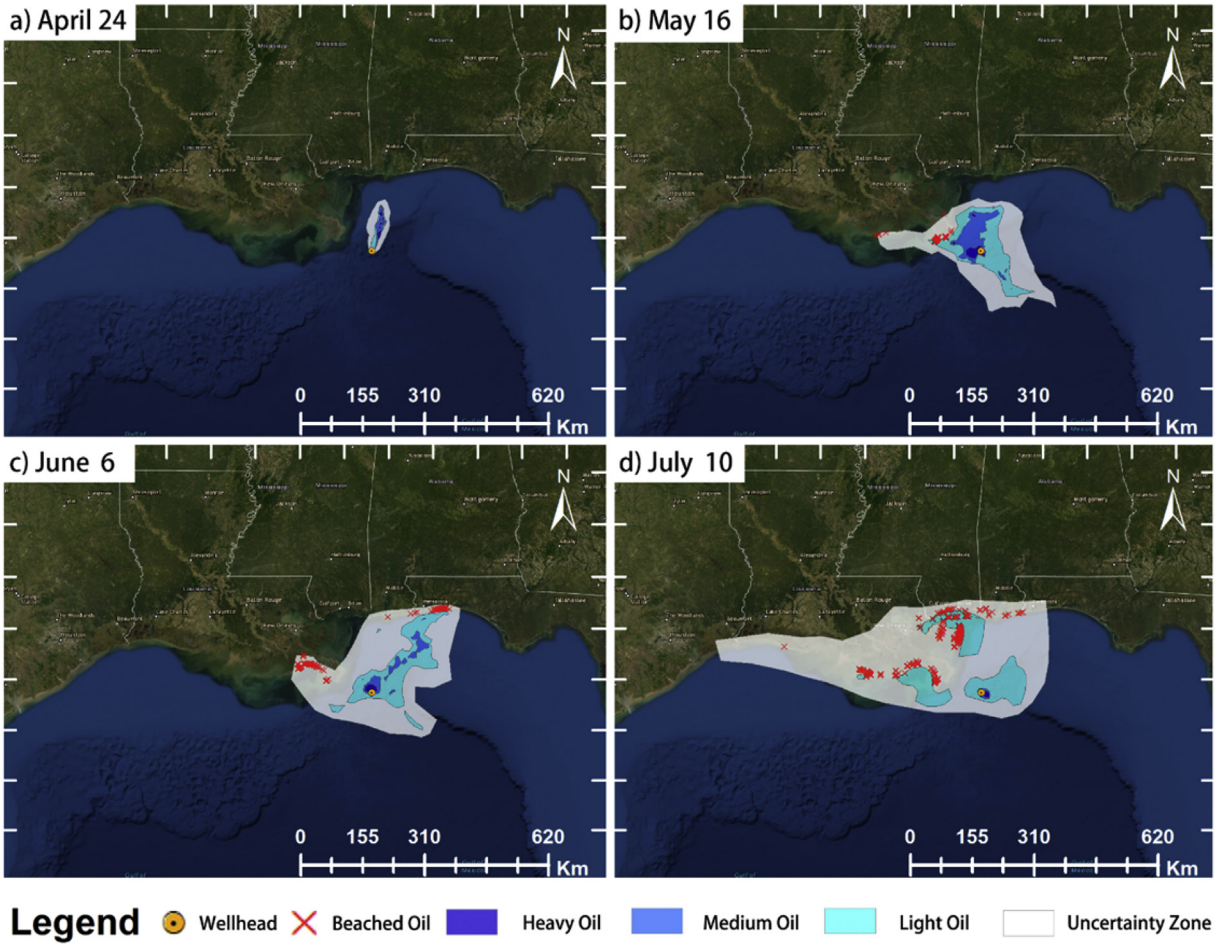

Fig. 1. Oil trajectory and beached oil simulated by the GNOME oil transport model for 24 April, 16 May, 6 June and 10 July.

chemical concentrations over periods of many days and so the continuity of the landfall signal was important for this method. The CCC method was then compared to oil spill trajectories as depicted by shoreline beaching and the oil impact zones generated through the GNOME model and as depicted by remote sensing imagery using SAR (Cheng et al., 2011).

To compare these methods, the focus area must be defined first. The area is to include the locations where the samples were collected, and the extent of the oil spill trajectories, as depicted from the GNOME oil transport model and from the SAR remote sensing images. Among the sample locations and trajectories, the sample locations had the widest range and so this range was used to define the spatial extent of the analysis, which corresponded to a latitude range of 1.5° (166.5 km) and a longitude sampling range of about 17.1° (1700.76 km). The longitude sampling range was one order of magnitude larger compared with the latitude range. Because of the large horizontal expanse of the sampling area, we chose to convert the 2-dimensional problem into a 1-dimensional problem by neglecting the latitude change. Thus, the longitude was used to assign a sampling point to a particular segment. Considering the density of the sampling points, the area where the largest density of data points was taken, from longitude −97 to −83, was split into 20 segments, where each segment length was 49.6 km (0.5°).

2.1. Trajectories and beached oil data from an oil transport model

The trajectories from the GNOME model provided two pieces of information, oil exposure zones and beached oil locations. The GNOME oil exposure zones (Fig. 1) include a dark blue region indicating heavy oil, a regular blue region indicating medium oil, a light blue region indicating light oil, and the white region indicating the uncertainty area. The uncertainty zone produced during response efforts corresponded to a combined output. This combined output was generated by applying GNOME using the results from several different hydrodynamic models, each utilizing wind and current data available from multiple sources. Each day during the spill, oil exposure zones were predicted using prior day's satellite imagery and daily predictions from the several available hydrodynamic models (Beegle-Krause, 2003). The intersection of the uncertainty zone with land was considered in the current study to represent the best estimate of the date of landfall from the oil exposure zones. The GNOME beaching algorithm checked whether the Lagranian elements between the prior simulated point location and the new point location encountered land. The exposure for a particular simulation date was then set (and shown by a red cross, see Fig. 1) if land was encountered. Oil trajectories showing exposure zones and beached oil from GNOME were available daily between 24 April to 31 July. The GNOME results for initial exposure dates were then compared to the results from the CCC method.

Oil footprints obtained from the GNOME oil transport model illustrate the evolution of the spill on a daily basis (Fig. 1). The first image (Fig. 1a) corresponds to 24 April, which is 4 days after the oil spill started. The oil leaked from the wellhead and was transported to the north. The second image (Fig. 1b) corresponds to 16 May, which is 26 days after the oil spill started. The oil continued leaking from the wellhead and covered a wider range. Most of the oil was transported to the east. Only a small amount of oil was transported to the west. Also, in this image the sites of landfall as predicted by the beaching algorithm are seen as bright red "X" symbols. The third image (Fig. 1c) corresponds to 6 June, which is 47 days after the oil spill. Most of the oil continued to move towards the east

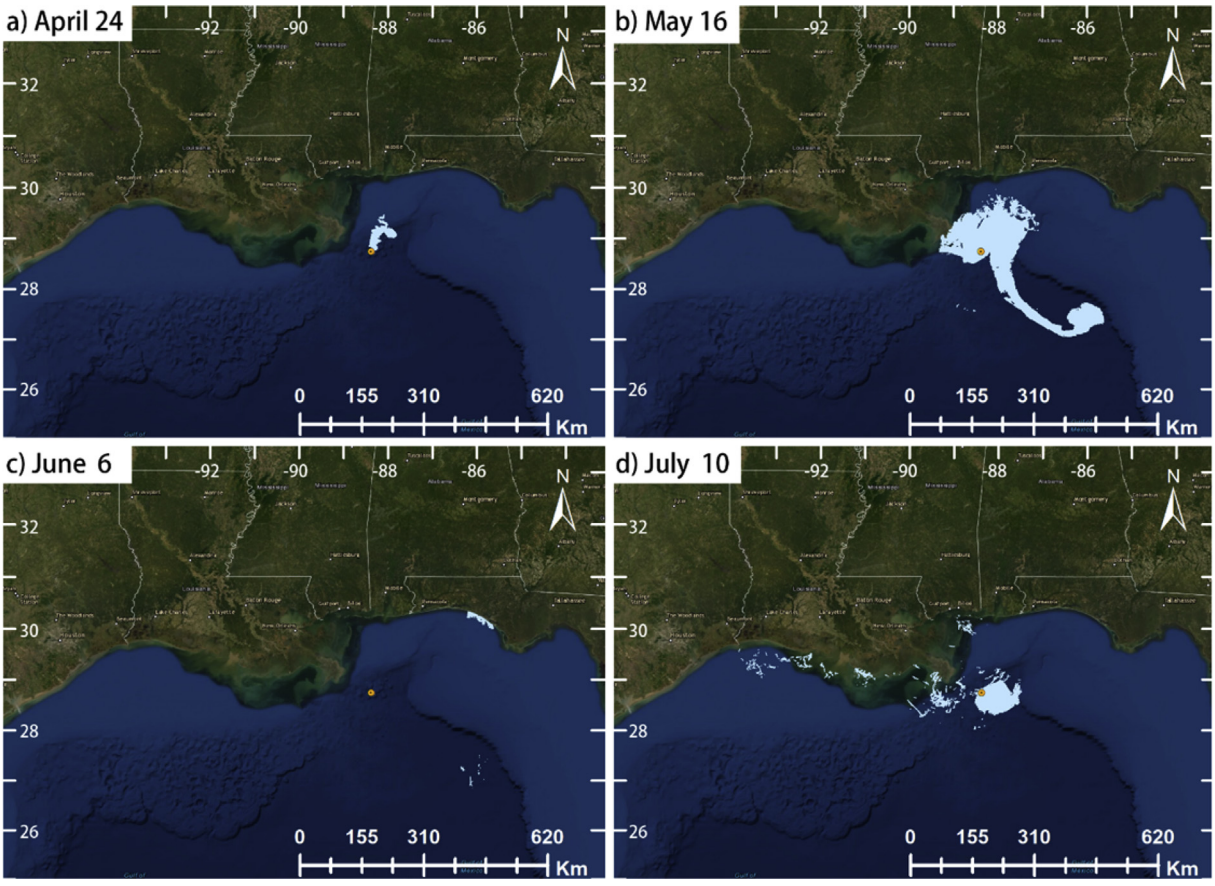

Fig. 2. Oil footprint interpreted from SAR remote sensing images for 24 April, 16 May, 6 June and 10 July.

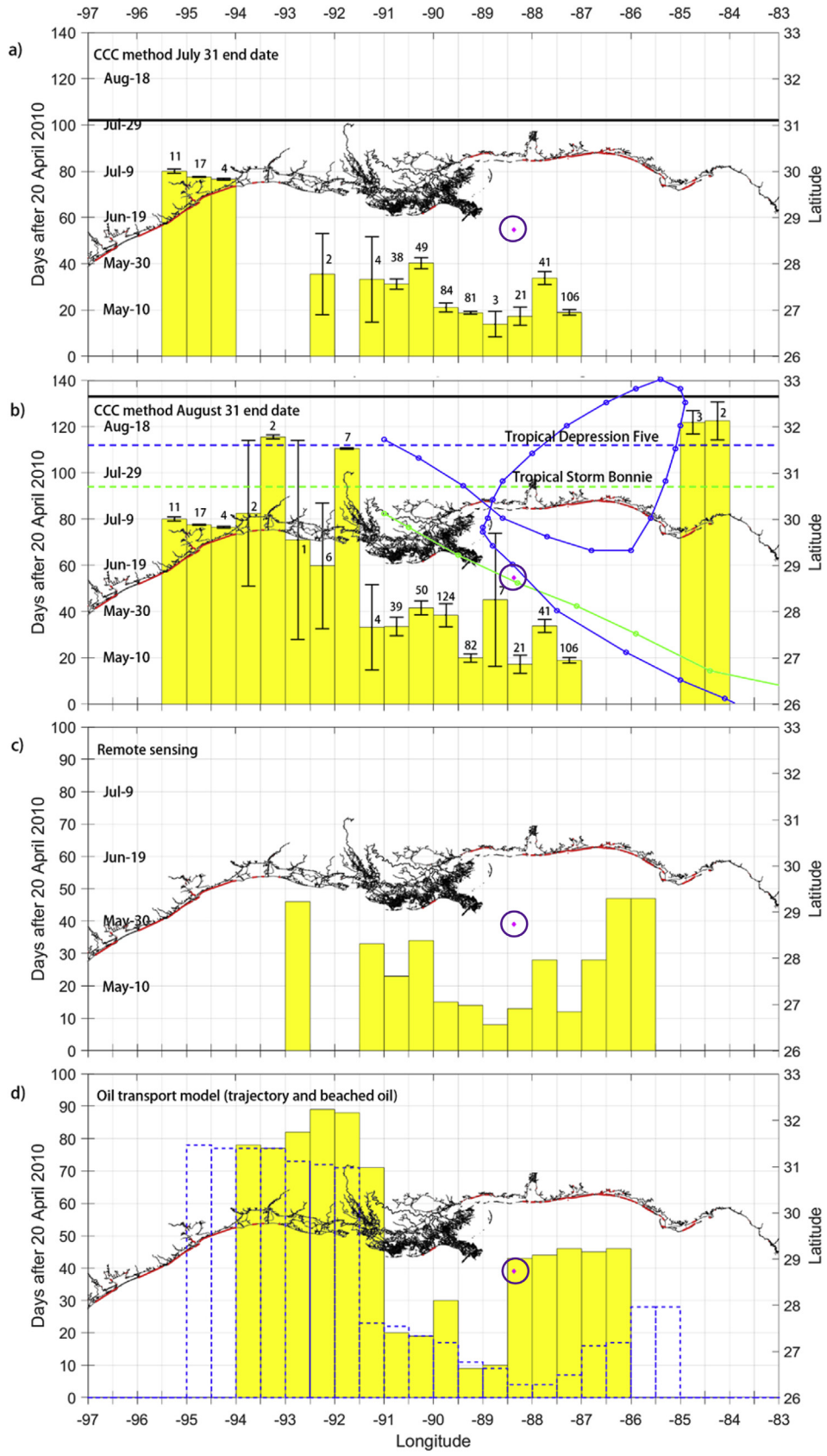

Fig. 3. Number of days after the oil spill (April 20, 2010) that the segment was exposed to oil based on the CCC method for the time period from April 20, 2010 to July 31, 2010 (panel a) and from April 20, 2010 to August 31, 2010 (panel b), remote sensing images (panel c) and oil spill transport model (panel d). The yellow bars in each panel indicate that the first oil exposure date for each segment and the purple rhombus surrounded by a circle shows the location of the wellhead. For panel a and b, the black solid line at the top of the panel means the end date of that group of data. The dashed lines with different colors indicate the date that tropical cyclones impacted the Gulf of Mexico. The paths of the cyclones are

Mobile Bay regions, with beaching predicted for the Mississippi delta and the eastern Alabama barrier islands. The west Mobile Bay regions were not exposed to the oil, according to the beached oil algorithm in GNOME. The fourth image (Fig. 1d) corresponds to 10 July, which is 81 days after the oil spill. At this time, the oil had started movement towards the west of GoM with beaching predicted in the Mississippi area, the west Mobile Bay regions and western tip of Florida.

2.2. Trajectories from remote sensing images

The remote sensing images of the oil footprint were downloaded from the ERMA (Environmental Response Management Application-Gulf of Mexico) website. These images were from Synthetic Aperture Radar (SAR) and interpreted with Textural Classifier Neural Network Algorithm (TCNNA). Similar to the output from the GNOME oil transport model, the oil footprints were evaluated in terms of the possible exposure of oil along the coast. For satellite data oil footprint data was available for a longer period of time, daily between 24 April to 10 August. Similar to the GNOME model results, a segment was regarded as exposed on the date the oil footprint overlapped the coast for that segment and these dates were then compared to the dates determined from the GNOME oil transport model and CCC method.

In Fig. 2, there are four images showing the oil footprint interpreted from remote sensing images, the dates of the images coinciding with those of Fig. 1. Similar to the GNOME oil transport results, the first image corresponding to 24 April (Fig. 2a), shows that the oil was transported to the north. The second image (Fig. 2b), corresponding to 16 May, shows the oil covering a wider range. Most of the oil was transported to the east in a similar fashion as predicted by GNOME. But in this case, more detail is available showing that the oil was entrained in the Loop Current frontal eddy, forming the distinctive “tiger tail” pattern. This observation was unique to the remote sensing observations. The third image (Fig. 2c) corresponds to 6 June. This date was chosen for illustration because it shows only a small amount of oil (in segments [-86, −85]), which indicates that the remote sensing image was not able to interpret the entire region on this day, especially given the comparative information from Fig. 1c corresponding to the GNOME results. It is highly likely that more oil was present in the region, but the remote sensing system was not able to capture the full extent of the oil spill on this day perhaps due to satellite paths and wave conditions. The fourth image (Fig. 2d) corresponds to 10 July, which is 81 days after the oil spill. The oil appears to have been transported towards the west at that time with significant detail in terms of the distribution of the oil in small strands and patches, a pattern that is distinctly different than the output from the GNOME oil transport model.

2.3. Computation of changes in OSC concentration data (CCC)

2.3.1. OSC concentration data set

Two large datasets were consolidated for the CCC analysis. These datasets are referred to as the U.S. Environmental Protection Agency (EPA) dataset and the Gulf of Mexico Research Initiative Information and Data Cooperative (GRIIDC) British Petroleum (BP) dataset. The EPA dataset contained 42,290 different measurements, with 14,433 measurements for sediment. Of the 14,433 measurements 2,032 were above the detection limits. This dataset mainly focused on the early exposure stages of the DWH oil spill, with sediment sampling dates ranging from April 30, 2010 to September 30, 2010. The GRIIDC-BP dataset contained merged data spanning April 29, 2010 to December 9, 2012 from 18 different named studies, and additional unnamed studies (See Tables S−1 in the supplement for details). This data set mainly focused on the late phases of the DWH oil spill. The total number of measurements in the GRIIDC-BP dataset was 794,543. The sediment data accounted for the majority (68%) of the dataset. Of the 540,659 measurements for sediments, about 65.7% were at or above detection limits, resulting in 355,213 data points for sediments above detection limits. In grand total, considering both the EPA and GRIIDC-BP datasets, a total of 357,245 data points were above detection limits for sediments.

This study focused on two data periods which showed distinct oil exposures to the coastline. The first period, April 20, 2010 to July 31, 2010 (period 1), corresponded primarily during the active spill period which continued through 15 July when the wellhead was capped. One tropical cyclone impacted the region towards the end of this period (Crone and Tolstoy, 2010; Curcic et al., 2016). During the following month, August, there was another major tropical cyclone after which additional oil exposures to the coastline were observed. To capture these cyclone-related effects, a second period of data analysis (period 2) was identified as 20 April to 31 August. In addition to the analysis periods and the −97 to −83 spatial extent of the focus area, data points were further constrained by the fact that specific chemicals were to have been measured multiple times during the analysis periods. Given these constraints, a total of 42,428 and 46,748 different measurements were available for analysis for period 1 and for period 2, respectively. The large decrease in number of measurements was due to the majority of GRIIDC-BP measurements after the target periods for this study. Although the EPA and GRIIDC-BP combined dataset included concentrations values for 293 different chemicals, this study utilized data for a subset of the chemicals (164) which met the time, spatial and multiple measures constraints. A list of the 164 chemicals is provided in Tables S−3 in the supplemental text.

2.3.2. CCC method description

By comparing the concentrations of one particular chemical between two consecutive sampling dates, the increase in concentration can be computed. The change in concentration was therefore used to indicate whether the coastal region was exposed to oil. A large increase indicated that the chemical impacted the region between the two sampling dates.

For each chemical for each day, the arithmetic mean of the sampling data within each segment was used as the concentration for the chemical in that segment. The second step was to calculate the increase, r, by the following equation: $r = \frac{C_2 - C_1}{C_1} * 100\%$ where C_1 was the concentration for the first date, $date_1$, which can be considered the background concentration. C_2 was the concentration for the second date, $date_2$, which is considered the concentration after the chemical impacted the region. The oil exposure date was between the first sampling date and the second sampling date. In this research, an increase by 100% (or a doubling of the concentration) was used as the threshold to identify an exposure.

shown in green (Tropical Storm Bonnie) and blue (Tropical Depression Five) in panels a and b. The error bars for each segment show the confidence range of the exposure dates for each segment. The number above the bar corresponds to the number of chemicals that were used to estimate the exposure date. For reference red lines across the coastline correspond to beach areas. The yellow bars in panel d indicate the result based on beached oil data and the blue dash lines indicates the result based on exposure zone trajectories from oil transport model. (For interpretation of the references to color in this figure legend, the reader is referred to the Web version of this article.)

After trying 50%, 100%, 150%, 200%, 250% and 300%, we found that the difference between results was relatively small (See supplement Tables S–4). Among the factors taken into consideration, there were two key factors which were used to decide upon the threshold value of 100%. The first factor was the number of chemicals identified as meeting the threshold. The more chemicals that met the threshold, the more evidence was available to support that an oil exposure occurred. The biggest difference in exposure dates when considering different threshold values was observed in segment [-91.5, −91]. When the threshold was set to 150%, the exposure date was computed at 21 days. When the threshold was set to 50% or 100%, the exposure date was computed at 33.3 days. The number of chemicals meeting the 50% and 100% threshold was 4, but the number of chemicals meeting the 150% threshold was only 2. The 50% and 100% thresholds were considered to be more reliable because of the greater number of chemicals meeting the threshold criteria. The second factor considered when deciding the threshold value was the background level of the chemicals. Among the 164 chemicals used in this research, many of them have very low background concentrations. For example, 13b(H),17a(H)-20S-Diacholestane, has a mean concentration of 0.02–0.04 μg/kg for different segments before the oil exposure date. Fluctuations of 50% may be reasonable (0.01–0.02 μg/kg) due to natural variability within background levels. When a choice was to be made, there was a tendency to err towards the larger threshold value as opposed to the lower threshold value due to natural variations in background concentrations. So a threshold value of 100% was chosen for the DWH case study.

For segments with more than two chemicals showing exposures, the distribution of dates ($date_1$ and $date_2$) was fitted according to the distribution of a student t-test. The exposure date was set to the mean of the distribution and the range of exposure dates (shown by error bars in Fig. 3a and b) was set to the 95% confidence limits. If the number of doubled chemicals was 2 or 1, the error bars corresponded to the actual sampling date range. The mean of the sampling date range was then used as the first exposure date of that segment.

3. Results and discussion

3.1. Results

The oil exposure date calculated from CCC method (Fig. 3a) based on the period 1 time range from April 20, 2010 to July 31, 2010 shows that the geographic range of the oil exposure was [-95.5, −87]. Among this range, segments [-94, −92.5] and [-92, −91.5] were not exposed to oil. Results also show that the earliest segment exposed to oil was [-89, −88.5]. The date was May 4, 2010, 14 days after the DWH explosion. The first exposure date for each segment increased with the distance to the east and west for segments [-95.5, −87] except segments [-90.5, −90] and [-88, −87.5]. In terms of the uncertainty range for the exposure date predictions, in general, the range of exposure date predictions was greater when the number of chemicals that doubled in concentration were smaller. This was observed for the first segment exposed [-89, −88.5] and also for the "gap" for segments between [-94, −91] where OSC exposures were not as pronounced, with only four chemicals that doubled for [-91.5,-91], and two for [-92.5, −92]. The exposure date range (error bar) is wide for these segments due limited chemical exposures in this region prior to July 31.

For the longer time range (period 2), from April 20, 2010 to August 31, 2010, the oil exposure date calculated from the CCC method (Fig. 3b) showed a wider range of exposures. For this case, exposures are now observed at all segments between [-94, −91.5]. Additionally, exposures are observed farther east at segments [-85, −84], with no exposure at segments [-87, −85]. Results also showed that the earliest segment exposed to oil was [-88.5, −88], corresponding to May 10, 2010, 20 days after the explosion. Similar to Fig. 3a, the first exposure date for each segment increased with the distance away from segment [-88.5, −88] except segments [-89, −88.5] and [-88, −87.5]. For segments [-91.5, −90.5], they have an earlier first exposure date. (The reason will be discussed in the discussion section). The green dash line corresponds to the track of Tropical Storm Bonnie which occurred 22–24 July 2010 and influenced the Mississippi Delta. The blue dash line corresponds to the track of Tropical Depression Five which occurred 10–11 August 2010 and influenced the middle and east GoM (Fig. 3a and b). Most of the new segments now show exposures (inclusive of dates indicated by error bars) near the dates of Tropical Depression Five. Similarly, for the CCC method for period 1, the number of chemicals (n) that doubled by the inclusion of the additional month of data during period 2 was relatively few. The new bars that "fill in the gap" on the west end of the target area either coincided with the date of Tropical Depression Five ([-92, −91.5] with n = 7, and [-93.5, −93] with n = 2) resulting in tight error bars or showed a more gradual increase in chemical concentrations for a few chemicals ([-92.5,-92] with n = 6, [-92.5,-93] with n = 1, and [-93.5,-93] with n = 2) resulting in a wider range in the error bars. The new exposure dates to the east [-85, −84] are consistent with one another although only a few chemicals showed a doubling of concentration as per CCC method (n of 3 and 2, respectively).

The oil exposure date interpreted from remote sensing images (Fig. 3c) shows exposures within segments [-93, −85.5]. The segment exposed the earliest was [-89, −88.5], corresponding to 28 April, 8 days after the explosion. In a similar fashion as for Fig. 3a and b, the first exposure date for each segment increased with the distance away from segments [-89, −88.5] except segment [-90.5, −90] and [-88, −87.5].

There were two results shown in Fig. 3d, which are shown by the yellow bar and the blue dash lines. The yellow bar corresponds to the beached oil data and the blue dash lines corresponds to the oil trajectories' exposure zones. The oil exposure date interpreted from beached oil (Fig. 3d) showed that the exposure range was [-94, −86]. The earliest impacted segment was [-89.5, −89], corresponding to 29 April, 9 days after the oil spill happened. For segment [-89, −88.5], its exposure date was 30 April. The coincidence in timing for these two segments was because of their close proximity to the wellhead, located near −89. The first segment exposed to oiling as predicted by the various methods could correspond to either segment depending upon assumptions due to the close proximity to the wellhead.

For predictions from the oil spill exposure zones (Fig. 3d), the results were different from the beached oil even though both were based upon the GNOME oil transport model. For the oil spill exposure zones, the area was wider [-95, −85] than predicted based on beached oil [-94, −86]. Additionally, the majority of the exposures were earlier in time.

3.2. Discussion

The earliest segment exposed to oil differed depending upon the method used. The result based on CCC method using period 1 indicated that segment [-89, −88.5] was the earliest exposed (May 4, 2010) segment (Fig. 3a). This result came from 3 chemicals (3 chemical concentrations doubled in the time range) and the error was relatively large, which means the result was reasonable but not conclusive. The result based on CCC method using period 2 indicated that the adjacent segment [-88.5,-88] was the earliest exposed (May 10, 2010) segment. It was six days later than the

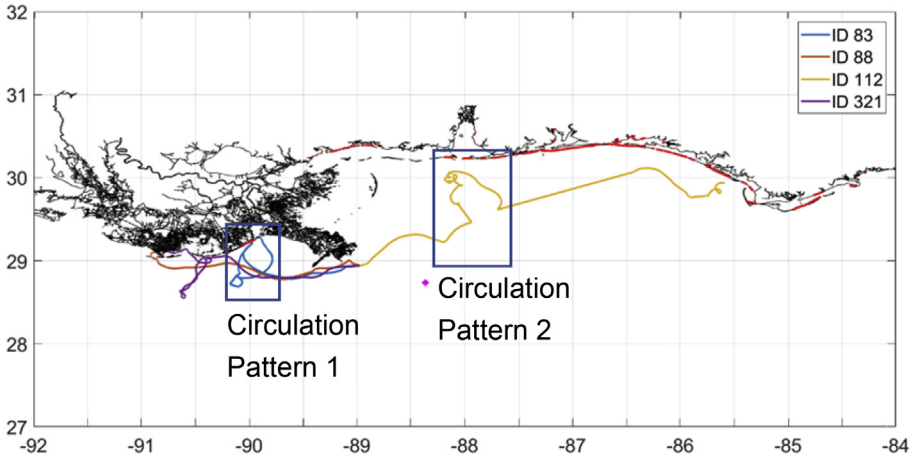

Fig. 4. Drifter trajectories. The data is from four undrogued CARTHE drifters. The drifters were launched offshore in segment [-89, −88.5] on April 20th, 2017.

earliest date calculated using period 1 for the adjacent segment. Interestingly, for this segment [-88.5,-88] the period 1 and period 2 analysis resulted in the same exposure date of May 10, 2010. The consistency in the date is influenced by the large number of chemicals that doubled for the period 1 analysis (n = 81) and period 2 analysis (n = 82). In essence the change in first exposure date was a result from segment [-89,-88.5] which during period 1 was characterized by 3 chemicals doubling in concentration and during period 2 with 7 chemicals doubling in concentration. This significant increase in the number of chemicals that doubled in concentration, from 3 to 7, drove the range of the first exposure date towards later times thereby delaying the estimated exposure date from May 4, 2010 to June 4, 2010.

4. Conclusion

We have developed a new method named chemical concentration change (CCC) method. The method is based upon identifying changes in chemical concentrations in nearshore areas to identify contaminant exposure dates. The method has several applications. It can be used to check the predictions of landfall dates as estimated through fate and transport models. Many fate and transport models are based upon offshore water conditions which may not be representative of nearshore conditions. The results from the CCC method can be used to determine whether these types of model assumptions are accurate. The CCC method can also be used to evaluate whether remote sensing images concur with measurements on the ground. The actual landfall date predictions from remote sensing images can be variable due to the fine spatial and temporal resolutions needed at the coastline to discern oil exposures, assuming they are visible. In addition, the CCC method is applicable to different types of contaminants, not only oil spill chemicals. For example, it can be used to evaluate the exposure dates from sewage spills, harmful algal blooms, floating debris, and other impacts to shorelines as long as data are available to confirm levels along the nearshore before and after exposure. Also differences between the CCC method and other methods can possibly elucidate oceanic processes which may have not been considered, such as the river-induced effect and the influence of tropical cyclones, which were not taken into consideration in GNOME model and were not obvious through remote sensing imagery.

Specifically using the data available through DWH, this method identified the first exposure date of oil within different regions along the GoM between longitude −97 to −83. For most of the

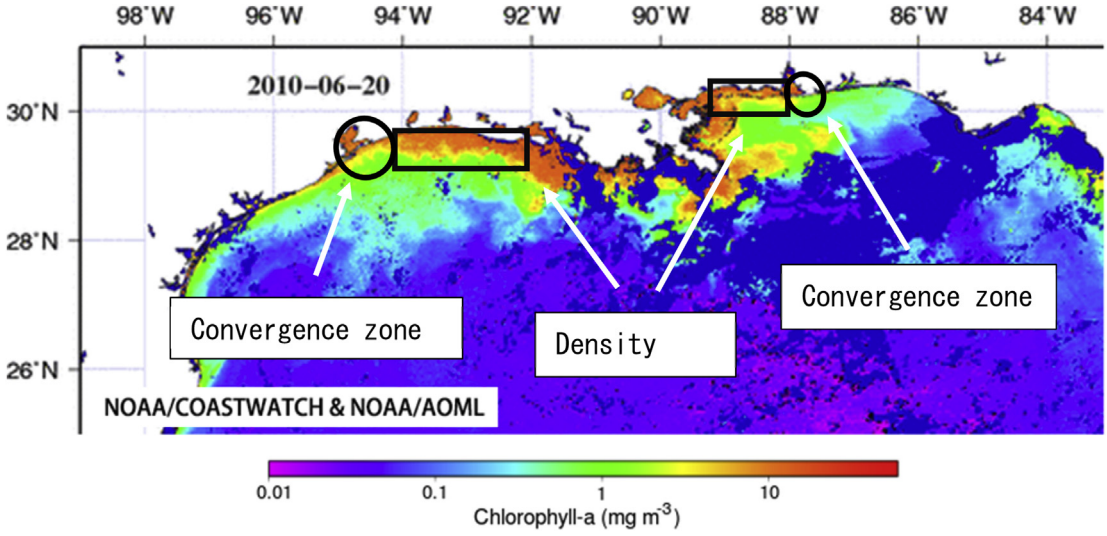

Fig. 5. Ocean Color (chlorophyll-*a*) map for Gulf of Mexico during June 8, 2010 and June 20, 2010. The color indicates the concentration of chlorophyll *a*. It is used to distinguish fresh water from sea water. The ocean color maps were downloaded from NOAA website (https://www.aoml.noaa.gov/phod/dhos/color.php). (For interpretation of the references to color in this figure legend, the reader is referred to the Web version of this article.)

segments between −91.5 and −87, the exposure date increased with distance away from the wellhead. There were two abnormal segments, segment [-90.5, −90] and segment [-88, −87.5], the dates were late compared with the adjacent segments. We hypothesize that this was due to the circulations caused by the fresh water from Mississippi River and Alabama River mixing with the sea water (Fig. 4, see circulation patterns 1 and 2). Segments [-94, −91] were less impacted by oil, which we hypothesize was due to the density fronts caused by the mixing of fresh water and saltwater (also known as the river induced effect) (Androulidakis et al., 2018; Kourafalou and Androulidakis, 2013) (Fig. 5). For segments [-94, −91], a great amount of fresh water from Mississippi River likely protected that region and oil was transported along the density fronts to the west, passing through and finally impacting segments [-95.5, −94]. In a similar fashion as for segment [-88, −87.5], oil transport along the density fronts to the east led to the late impact, and finally impacting segment [-87.5, −87]. The large number of chemicals for this segment (106) we believe may have been due to the convergence zone of freshwater along the coast allowing oil to hit the coastline in that segment and leaving areas farther east without oil impacts.

There were two cyclones that occurred immediately after the oil spill which influenced oil transport. First were segments [-85, −84]. Based on CCC method, these segments were not impacted in July, but were impacted in August. According to Tropical Depression Five's date and trajectories, it is likely that the impact was due to the cyclone. The second influence was that for segments [-90, −89.5] and [-89, −88.5], showing that the number of chemicals whose concentration doubled was increased. This meant that there were additional hits in August in those segments. The wellhead was capped at July 15, 2010, which meant that the additional oil hit those regions was not directly from the wellhead.

CRediT authorship contribution statement

Junfei Xia: Conceptualization, Methodology, Software, Validation, Formal analysis, Writing - original draft, Visualization. **Wei Zhang:** Conceptualization, Methodology, Writing - review & editing. **Alesia C. Ferguson:** Conceptualization, Writing - review & editing. **Kristina D. Mena:** Conceptualization, Writing - review & editing. **Tamay M. Özgökmen:** Conceptualization, Methodology, Writing - review & editing. **Helena M. Solo-Gabriele:** Conceptualization, Methodology, Writing - review & editing, Project administration, Funding acquisition.

Acknowledgements

This research was made possible by a grant from The Gulf of Mexico Research Initiative. Data are publicly available through the Gulf of Mexico Research Initiative Information & Data Cooperative (GRIIDC) at https://data.gulfresearchinitiative.org (doi:10.7266/4DEHBK1A).

Appendix A. Supplementary data

Supplementary data to this article can be found online at https://doi.org/10.1016/j.envpol.2019.113858.

References

Al-Majed, A.A., Adebayo, A.R., Hossain, M.E., 2012. A sustainable approach to controlling oil spills. J. Environ. Manag. 113, 213–227.

Androulidakis, Y., Kourafalou, V., Özgökmen, T., Garcia-Pineda, O., Lund, B., Le Hénaff, M., Hu, C., Haus, B.K., Novelli, G., Guigand, C., Kang, H., 2018. Influence of river-induced fronts on hydrocarbon transport: a multiplatform observational study. J. Geophys. Res.: Oceans 123 (5), 3259–3285.

Bae, H.S., Huang, L., White, J.R., Wang, J., DeLaune, R.D., Ogram, A., 2018. Response of microbial populations regulating nutrient biogeochemical cycles to oiling of coastal saltmarshes from the Deepwater Horizon oil spill. Environ. Pollut. 241, 136–147.

Beegle-Krause, C.J., 1999. GNOME: NOAA's next-generation spill trajectory model. Oceans' 99. MTS/IEEE. Riding the Crest into the 21st Century. Conference and Exhibition. In: Conference Proceedings (IEEE Cat. No. 99CH37008), vol. 3. IEEE, pp. 1262–1266.

Beegle-Krause, C.J., 2003. Advantages of separating the circulation model and trajectory model: GNOME trajectory model used with outside circulation models. In: Arctic and Marine Oil Spill Program Technical Seminar, vol. 2. Environment Canada, pp. 825–840, 1999.

Beegle-Krause, J., 2001. General NOAA oil modeling environment (GNOME): a new spill trajectory model. In: International Oil Spill Conference, vol. 2001. American Petroleum Institute, pp. 865–871. No. 2.

Berta, M., Griffa, A., Magaldi, M.G., Özgökmen, T.M., Poje, A.C., Haza, A.C., Olascoaga, M.J., 2015. Improved surface velocity and trajectory estimates in the Gulf of Mexico from blended satellite altimetry and drifter data. J. Atmos. Ocean. Technol. 32 (10), 1880–1901.

Black, J., Welday, J., Buckley, B., Ferguson, A., Gurian, P., Mena, K., Yang, I., McCandlish, E., Solo-Gabriele, H., 2016. Risk assessment for children exposed to beach sands impacted by oil spill chemicals. Int. J. Environ. Res. Public Health 13 (9), 853.

Cheng, Y., Li, X., Xu, Q., Garcia-Pineda, O., Andersen, O.B., Pichel, W.G., 2011. SAR observation and model tracking of an oil spill event in coastal waters. Mar. Pollut. Bull. 62 (2), 350–363.

Crone, T.J., Tolstoy, M., 2010. Magnitude of the 2010 Gulf of Mexico oil leak. Science 330 (6004), 634-634.

Curcic, M., Chen, S.S., Özgökmen, T.M., 2016. Hurricane-induced ocean waves and Stokes drift and their impacts on surface transport and dispersion in the Gulf of Mexico. Geophys. Res. Lett. 43 (6), 2773–2781.

Freudenburg, W.R., Gramling, R., 2011. Blowout in the Gulf: the BP Oil Spill Disaster and the Future of Energy in America. MIT Press.

Ganta, R.R., Zaheeruddin, S., Baddiri, N., Rao, R.R., 2012. Segmentation of oil spill images with illumination-reflectance based adaptive level set model. IEEE J. Sel. Top. Appl. Earth Obs. Rem. Sens. 5 (5), 1394–1402.

Garcia-Pineda, O., MacDonald, I.R., Li, X., Jackson, C.R., Pichel, W.G., 2013. Oil spill mapping and measurement in the Gulf of Mexico with textural classifier neural network algorithm (TCNNA). IEEE J. Sel. Top. Appl. Earth Obs. Rem. Sens. 6 (6), 2517–2525.

Garcia-Pineda, O., Zimmer, B., Howard, M., Pichel, W., Li, X., MacDonald, I.R., 2009. Using SAR images to delineate ocean oil slicks with a texture-classifying neural network algorithm (TCNNA). Can. J. Remote Sens. 35 (5), 411–421.

Hamilton, P., Donohue, K.A., Leben, R.R., Lugo-Fernández, A., Green, R.E., 2011. Loop current observations during spring and summer of 2010: description and historical perspective. Monitoring and modeling the deepwater Horizon oil spill: a record-breaking enterprise. Geophys. Monogr. Ser. 195, 117–130.

Kourafalou, V.H., Androulidakis, Y.S., 2013. Influence of Mississippi River induced circulation on the Deepwater Horizon oil spill transport. J. Geophys. Res.: Oceans 118 (8), 3823–3842.

Kujawinski, E.B., Kido Soule, M.C., Valentine, D.L., Boysen, A.K., Longnecker, K., Redmond, M.C., 2011. Fate of dispersants associated with the Deepwater Horizon oil spill. Environ. Sci. Technol. 45 (4), 1298–1306.

Le Hénaff, M., Kourafalou, V.H., Paris, C.B., Helgers, J., Aman, Z.M., Hogan, P.J., Srinivasan, A., 2012. Surface evolution of the Deepwater Horizon oil spill patch: combined effects of circulation and wind-induced drift. Environ. Sci. Technol. 46 (13), 7267–7273.

Leifer, I., Lehr, W.J., Simecek-Beatty, D., Bradley, E., Clark, R., Dennison, P., Hu, Y., Matheson, S., E Jones, S., Holt, B., Reif, M., 2012. State of the art satellite and airborne marine oil spill remote sensing: application to the BP Deepwater Horizon oil spill. Remote Sens. Environ. 124, 185–209.

Liu, Y., MacFadyen, A., Ji, Z.G., Weisberg, R.H. (Eds.), 2013. Monitoring and Modeling the Deepwater Horizon Oil Spill: a Record Breaking Enterprise, vol. 195. John Wiley & Sons.

McCready, D., Williams, J.B., 2011. A simplified approach to evaluate human and aquatic exposure to a chemical spilled in a river. J. Hazard Mater. 193, 225–232.

McNutt, M.K., Camilli, R., Crone, T.J., Guthrie, G.D., Hsieh, P.A., Ryerson, T.B., Savas, O., Shaffer, F., 2012. Review of flow rate estimates of the Deepwater Horizon oil spill. Proc. Natl. Acad. Sci. 109 (50), 20260–20267.

Michel, J., Owens, E.H., Zengel, S., Graham, A., Nixon, Z., Allard, T., Holton, W., Reimer, P.D., Lamarche, A., White, M., Rutherford, N., 2013. Extent and degree of shoreline oiling: Deepwater Horizon oil spill, Gulf of Mexico, USA. PLoS One 8 (6), e65087.

Özgökmen, T.M., Beron-Vera, F.J., Bogucki, D., Chen, S.S., Dawson, C., Dewar, W., Griffa, A., Haus, B.K., Haza, A.C., Huntley, H., Iskandarani, M., 2014. Research overview of the consortium for advanced research on transport of hydrocarbon in the environment (CARTHE). In: International Oil Spill Conference Proceedings, vol. 2014. American Petroleum Institute, pp. 544–560. No. 1.

Özgökmen, T.M., Chassignet, E.P., Dawson, C.N., Dukhovskoy, D., Jacobs, G., Ledwell, J., Garcia-Pineda, O., MacDonald, I.R., Morey, S.L., Olascoaga, M.J., Poje, A.C., 2016. Over what area did the oil and gas spread during the 2010 Deepwater Horizon oil spill? Oceanography 29 (3), 96–107.

Price, J.M., Reed, M., Howard, M.K., Johnson, W.R., Ji, Z.G., Marshall, C.F., Guinasso Jr., N.L., Rainey, G.B., 2006. Preliminary assessment of an oil-spill trajectory model using satellite-tracked, oil-spill-simulating drifters. Environ.

Model. Softw 21 (2), 258–270.
Smith, R.H., Johns, E.M., Goni, G.J., Trinanes, J., Lumpkin, R., Wood, A.M., Kelble, C.R., Cummings, S.R., Lamkin, J.T., Privoznik, S., 2014. Oceanographic conditions in the Gulf of Mexico in July 2010, during the deepwater Horizon oil spill. Cont. Shelf Res. 77, 118–131.
Walker, N.D., Pilley, C.T., Raghunathan, V.V., D'Sa, E.J., Leben, R.R., Hoffmann, N.G., Brickley, P.J., Coholan, P.D., Sharma, N., Graber, H.C., Turner, R.E., 2011. Impacts of Loop current frontal cyclonic eddies and wind forcing on the 2010 Gulf of Mexico oil spill. Monitoring and modeling the deepwater Horizon oil spill: a record-breaking enterprise. Geophys. Monogr. Ser. 195, 103–116.
Xu, Q., Zheng, J., Cheng, Y., Zhang, S., Chen, M., Huang, Q., 2016. Detection of marine oil spills from SAR images using artificial neural networks. In: The 26th International Ocean and Polar Engineering Conference. International Society of Offshore and Polar Engineers.